JOC Article

Structures of 1-(Arylseleninyl)naphthalenes: O, G, and Y Dependences in 8-G-1-[*p*-$YC_6H_4Se(O)$]$C_{10}H_6$

Satoko Hayashi, Hideki Wada, Takashi Ueno, and Waro Nakanishi*

Department of Material Science and Chemistry, Faculty of Systems Engineering, Wakayama University, 930 Sakaedani, Wakayama 640-8510, Japan

nakanisi@sys.wakayama-u.ac.jp

Received March 10, 2006

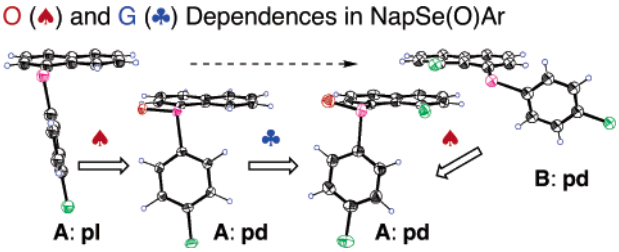

Structures of 8-G-1-[*p*-$YC_6H_4Se(O)$]$C_{10}H_6$ [**1** (G = H), **2** (G = F), **3** (G = Cl), and **4** (G = Br): Y = H, OMe, OCH_2Ph, *t*-Bu, Me, Cl, and NO_2] and $(1\text{-}C_{10}H_7)_2SeO$ (**5**) are investigated by the X-ray crystallographic analysis. Structures of **1** are all **A** with regard to the naphthyl group (**1** (**A**)), where the Se−C_{Ar} and Se−O bonds are perpendicular to and parallel to the naphthyl plane, respectively. Those of **2**−**4** are also **A**. Since structures of 8-G-1-(*p*-$YC_6H_4Se)C_{10}H_6$ [**7** (G = F), **8** (G = Cl), and **9** (G = Br)] are all **B**, the results exhibit that **B** of **7**−**9** change dramatically to **A** of **2**−**4** with the introduction of O atoms. The factor to determine the **A** structures of **1**−**4** by O is called O dependence. The origin of the O dependence is the nonbonded n_p(O)- - -π(Nap) interaction, which results in CT from n_p(O) to π(Nap) since O in **1**−**4** is highly electron rich due to the polar $Se^+{=}O^-$ bond and π(Nap) acts as an acceptor. There are two types of n_p(O)'s, n_{py}(O) and n_{pz}(O), if the directions of the Se−O bond and the p-orbitals of π(Nap) are taken in the *x*- and *z*-axes, respectively. Double but independent n_p(O)- - -π(Nap) interactions in **5** lead to **5** (**AA**). The conformation of the *p*-YC_6H_4Se group in **1** changes depending on Y (Y dependence), although the effect is not strong. The Y dependence is explained on the basis of the magnitude of CT of the n_p(O)→π(Ar) type in **1**, in addition to the n_p(O)- - -π(Nap) interaction. The structure around the Se═O group in **1** is close to that of **5** (**AA**), if the accepting ability of the *p*-YC_6H_4Se group is similar to that of the naphthyl group. **A** of **2**−**4** are further stabilized by the n_p(G)- - -σ^*(Se−O) 3c−4e interactions, which are called G dependence. QC calculations performed on the methyl analogues of **1**−**4** (**11**−**14**, respectively) reproduced the observed structures, supported the above discussion, and revealed the energy profiles. The energy-lowering effect of the O dependence would be close to the G dependence of the nonbonded n(Br)- - -σ^*(Se−O) 3c−4e interaction in **14** if the steric repulsion between Br and Se is contained in the G dependence. The value is roughly predicted as 20 kJ mol^{-1}. The structures of **1**−**5** are well explained by O, G, and Y dependences.

Introduction

Weak interactions are of current interest.[1−6] They can be used to determine the fine structures of compounds. However, it is sometimes difficult to detect the interactions and/or explain the phenomena arising from them, under the physical necessity, since weak interactions are usually literally very weak. Therefore, our investigations are focused to the phenomena arising from the direct orbital overlaps containing lone pair orbitals of group 16 elements.[4] Naphthalene 1,8-positions supply a good

* To whom correspondence should be addressed. Tel: +81 73 457 8252. Fax: +81 73 457 8253.

(1) (a) *Molecular Interactions. From van der Waals to Strongly Bound Complexes*; Scheiner, S., Ed.; Wiley: New York, 1997. (b) Asmus, K. D. *Acc. Chem. Res.* **1979**, *12*, 436−442. (c) Musker, W. K. *Acc. Chem. Res.* **1980**, *13*, 200−206.

10.1021/jo060527f CCC: $33.50
Published on Web 06/17/2006

system to investigate such interactions, since the distances between the nonbonded atoms at the 1,8-positions are close to the sum of van der Waals radii minus 1.0 Å.[4b,d−f,h,7]

Selenoxides [RSe(O)R′] afford optically active enantiomers, if R and R′ are not the same, since Se in each selenoxide is three-coordinated containing a lone pair.[8] Some efforts have been made to improve the utility of selenoxides as the starting compounds to introduce optical activity in a target molecule,[9,10] although the racemization of optically active selenoxides is usually very fast. The chemistry of selenoxides,[8] as well as sulfoxides,[11,12] has been widely studied; however, the structures of selenoxides are not well specified.[13,14] The factors that operate to control the fine structures of selenoxides have been elucidated, exemplified by 1-(arylseleninyl)naphthalenes and the derivatives bearing G at the 8-positions (8-G-1-[*p*-$YC_6H_4Se(O)$]$C_{10}H_6$ (8-G-1-[ArSe(O)]Nap): **1** (G = H), **2** (G = F), **3** (G = Cl), and **4** (G = Br); Y = H (**a**), OMe (**b**), OCH_2Ph (**b′**), *t*-Bu (**c**), Me (**d**), Cl (**e**), and NO_2 (**f**)) (Chart 1). Factors to control the fine structures of **1**−**4** and 1,1′-dinaphthyl selenoxide (**5**) have been clarified by examining the structures determined by the X-ray crystallographic analysis and by analyzing them on the basis of quantum chemical (QC) calculations.

CHART 1

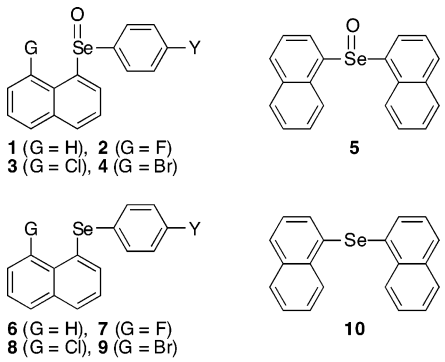

	a	b	b'	c	d	e	f
Y =	H	OMe	OCH_2Ph	Bu-*t*	Me	Cl	NO_2

The structures around the naphthyl group in 8-G-1-(*p*-$YC_6H_4Se)C_{10}H_6$ [**6** (G = H), **7** (G = F), **8** (G = Cl), and **9** (G = Br)] are well explained by types **A** (**A**), **B** (**B**), and **C** (**C**).[4c,d,f−h,5b] Similarly, those around the Ar group are classified by planar (**pl**), perpendicular (**pd**), and nonplanar and nonperpendicular (**np**) conformers,[4c−e,g,h,5b,15] although they might change successively. Scheme 1 shows the structures of **1**−**4** and **6**−**8**; the notation is employed throughout the text. The characters in the structures of **6**−**8** are summarized as follows: the structures of **6** are **A** if Y are acceptors such as Cl, Br, COOEt, and NO_2, whereas they are **B** when Y are donors such as OMe (Y dependence).[5b] Structures of **8** and **9** in Chart 1 are all **B**, as is **7b** (G dependence).[4h] While the origin of the Y dependence in **6** is the p−π conjugation of the n_p(Se)−π(Nap) and n_p(Se)−π(Ar) types, the G dependence in **7**−**9** is controlled by the nonbonded n_p(G)- - -σ^*(Se−C) 3c−4e interaction. The interaction aligns the three G- - -Se−C atoms linearly. The factors to control the structures of **1**−**5** will be clarified similarly to the cases of the Y and G dependences in **6**−**9**.[4h,5b]

Here, we report the fine structures of **1**−**5** bearing various substituents Y at the phenyl *p*-positions. The factors to control the structures are also elucidated, which are called O, Y, and G dependences in **1**−**5**, after the Y and G dependences in **6**−**9**.[4h,5b] All structures regarding to the naphthyl group in **1**−**4** are **A**, where the Se−C_{Ar} and Se−O bonds are perpendicular to and

(2) (a) Glass, R. S.; Andruski, S. W.; Broeker, J. L. *Rev. Heteroatom Chem.* **1988**, *1*, 3. (b) Glass, R. S.; Andruski, S. W.; Broeker, J. L.; Firouzabadi, H.; Steffen, L. K.; Wilson, G. S. *J. Am. Chem. Soc.* **1989**, *111*, 4036−4045. (c) Glass, R. S.; Adamowicz, L.; Broeker, J. L. *J. Am. Chem. Soc.* **1991**, *113*, 1065−1074.

(3) (a) Fujihara, H.; Ishitani, H.; Takaguchi, Y.; Furukawa, N. *Chem. Lett.* **1995**, 571−572. (b) Furukawa, N. *Bull. Chem. Soc. Jpn.* **1997**, *70*, 2571−2591. (c) Furukawa, N.; Kobayashi, K.; Sato, S. *J. Organomet. Chem.* **2000**, *611*, 116−126.

(4) (a) Nakanishi, W. *Chem. Lett.* **1993**, 2121−2122. (b) Nakanishi, W.; Hayashi, S.; Toyota, S. *Chem. Commun.* **1996**, 371−372. (c) Nakanishi, W.; Hayashi, S.; Yamaguchi, H. *Chem. Lett.* **1996**, 947−948. (d) Nakanishi, W.; Hayashi, S.; Sakaue, A.; Ono, G.; Kawada, Y. *J. Am. Chem. Soc.* **1998**, *120*, 3635−3640. (e) Nakanishi, W.; Hayashi, S.; Toyota, S. *J. Org. Chem.* **1998**, *63*, 8790−8800. (f) Hayashi, S.; Nakanishi, W. *J. Org. Chem.* **1999**, *64*, 6688−6696. (g) Nakanishi, W.; Hayashi, S.; Uehara, T. *J. Phys. Chem. A* **1999**, *103*, 9906−9912. (h) Nakanishi, W.; Hayashi, S. *J. Org. Chem.* **2002**, *67*, 38−48.

(5) (a) Nakanishi, W.; Hayashi, S.; Kihara, H. *J. Org. Chem.* **1999**, *64*, 2630−2637. (b) Nakanishi, W.; Hayashi, S.; Uehara, T. *Eur. J. Org. Chem.* **2001**, *2001*, 3933−3943.

(6) (a) Iwaoka, M.; Tomoda, S. *J. Am. Chem. Soc.* **1994**, *116*, 4463−4464. (b) Iwaoka, M.; Tomoda, S. *J. Am. Chem. Soc.* **1996**, *118*, 8077−8084. (c) Iwaoka, M.; Komatsu, H.; Tomoda, S. *Chem. Lett.* **1998**, 581−582. (d) Komatsu, H.; Iwaoka, M.; Tomoda, S. *Chem. Commun.* **1999**, 205−206.

(7) (a) Gafner, G.; Herbstein, F. H. *Acta Crystallogr.* **1962**, *15*, 1081−1092. (b) Davydova, M. A.; Struchkow, Yu. T. *Zh. Strukt. Kim.* **1962**, *3*, 184. (c) Davydova, M. A.; Struchkow, Yu. T. *Zh. Strukt. Kim.* **1968**, *9*, 1968. (d) Bock, H.; Sievert, M.; Havlas, Z. *Chem. Eur. J.* **1998**, *4*, 677−685. (e) Jackson, R. D.; James, S.; Orpen, A. G.; Pringle, P. G. *J. Organomet. Chem.* **1993**, *458*, C3−C4.

(8) (a) *The Chemistry of Organic Selenium and Tellurium Compounds*; Patai, S., Rappoport, Z., Eds.; John Wiley and Sons: New York, 1986; Vol. 1. (b) *The Chemistry of Organic Selenium and Tellurium Compounds*; Patai, S., Ed.; John Wiley and Sons: New York, 1986; Vol. 2. (c) *Organic Selenium Compounds: Their Chemistry and Biology*: Klayman, D. L., Günther, W. H. H., Eds.; Wiley: New York, 1973. (d) *Organic Selenium Chemistry*; Liotta, D., Ed.; Wiley-Interscience: New York, 1987. (e) *The Organic Chemistry of Tellurium*; Irgolic, K. J., Ed.; Gordan and Breach Science Publishers: New York, 1974. (f) *Organoselenium Chemistry, A practical Approach*; Back, T. G., Ed.; Oxford University Press: Oxford, 1999. See also references cited therein.

(9) (a) Drabowicz, J. *Hypervalent Sulfuranes as Transient and Isolable Structures: Occurrence, Synthesis, and Reactivity in Chemistry of Hypervalent Compounds*; Akiba, K.-y., Ed.; Wiley-VCH: New York, 1999; Chapter 7. (b) Drabowicz, J. *Heteroatom Chem.* **2002**, 5, 437−442.

(10) (a) Taka, H.; Matsumoto, A.; Shimizu, T.; Kamigata, N. *Chem. Lett.* **2000**, 726−727. (b) Taka, H.; Matsumoto, A.; Shimizu, T.; Kamigata, N. *Heteroatom Chem.* **2001**, *12*, 227−237. (c) Shimizu, T.; Enomoto, M.; Taka, H.; Kamigata, N. *J. Org. Chem.* **1999**, *64*, 8242−8247. (d) Nakashima, Y.; Shimizu, T.; Hirabayashi, K.; Iwasaki, F.; Yamasaki, M.; Kamigata, N. *J. Org. Chem.* **2005**, *70*, 5020−5027. (e) Fueno, H.; Ikuta, S.; Matsuyama, H.; Kamigata, N. *J. Chem. Soc., Perkin Trans. 2* **1992**, 1925−1928. (f) Kamigata, N.; Shimizu, T. *Rev. Heteroatom Chem.* **1991**, *4*, 226. (g) Rayner, D. R.; Gordon, A. J.; Mislow, K. *J. Am. Chem. Soc.* **1968**, *90*, 4854−4860.

(11) (a) *Organic Chemistry of Sulfur*: Oae, S., Ed.; Plenum Press: New York, 1977. (b) *Organic Sulfur Chemistry: Theoretical and Experimental Advances*; Bernardi, F., Csizmadia, I. G., Mangini, A., Eds.; Elsevier: Amsterdam, 1985.

(12) (a) Nakamura, S.; Yasuda, H.; Toru, T. *Tetrahedron: Asymmetry* **2002**, *13*, 1509−1518. (b) Nakamura, S.; Yasuda, H.; Watanabe, Y.; Toru, T. *J. Org. Chem.* **2000**, *65*, 8640−8650. (c) Nakamura, S.; Yasuda, H.; Watanabe, Y.; Toru, T. *Tetrahedron Lett.* **2000**, *41*, 4157−4160.

(13) (a) Takahashi, T.; Kurose, N.; Kawanami, S.; Arai, Y.; Koizumi, T. *J. Org. Chem.* **1994**, *59*, 3262−3264. (b) Procter, D. J.; Rayner, C. M. *Tetrahedron Lett.* **1994**, *35*, 1449−1452.

(14) (a) Jovanovic, M. V.; de Meester, P.; Biehl, E. R.; Chu, S. S. C. *J. Heterocycl. Chem.* **1986**, *23*, 801−807. (b) Tokunoh, R.; Sodeoka, M.; Aoe, K.-I.; Shibasaki, M. *Tetrahedron Lett.* **1995**, *36*, 8035−8038. (c) Kimura, T.; Izumi, Y.; Furukawa, N.; Minoshima, Y. *Heteroat. Chem.* **1996**, *7*, 143−147. (d) Bower, J. F.; Martin, C. J.; Rawson, D. J.; Slawin, A. M. Z.; Williams, J. M. J. *J. Chem. Soc., Perkin Trans. 1* **1996**, 333−342. (e) Nagy, P.; Csampai, A.; Szabo, D.; Varga, J.; Harmat, V.; Ruff, F.; Kucsman, A. *J. Chem. Soc., Perkin Trans. 2* **2001**, 339−349. (f) Reichardt, C.; Erfurt, H.-P.; Harms, K.; Schafer, G. *Eur. J. Org. Chem.* **2002**, 439−452.

SCHEME 1. Structures around Naphthyl and Aryl Groups in 8-G-1-[*p*-YC$_6$H$_4$Se(X)]C$_{10}$H$_6$, Where X = O for 1−4 and X = Null for 6−8

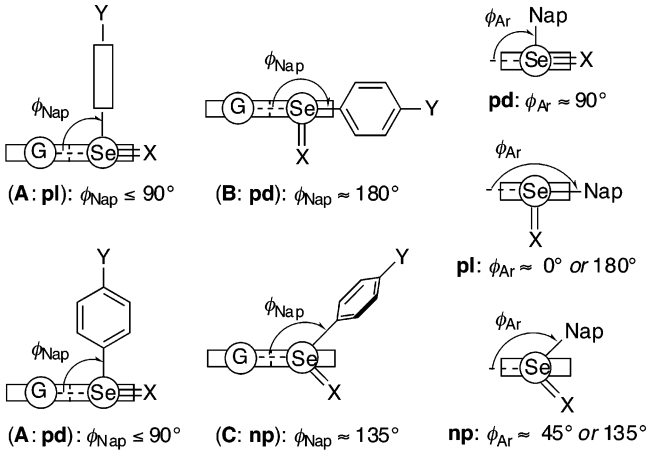

parallel to the naphthyl plane, respectively. This means that the **B** structure of **6b** (**6b** (**B**)) dramatically changes to **1b′** (**A**) with O introduced at Se, and **B** in **7**−**9** also change dramatically to **A** in **2**−**4**, with O for each. The structure of **1b′** (**A**) (Y = OCH_2Ph), instead of **1b** (Y = OMe), is discussed here, since crystals suitable for X-ray analysis are not obtained for **1b**.[16] The structural change by O at Se is called O dependence. Torsional angles (ϕ) around Se−C_{Ar} in **1** also change depending on Y, although not strongly, which is called Y dependence. While **A** in **1** are stabilized only by the O dependence, **A** in **2**−**4** bearing G of halogens at the 8-positions are stabilized through the n_p(G)- - -σ*(Se−O) 3c−4e interaction, in addition to the O dependence. We call it G dependence. QC calculations are employed to analyze the observed structures and to clarify the origin of the O and G dependences.

It is clarified how fine structures are controlled by weak interactions, exemplified by the selenoxides, which can be applied to other compounds. It can provide basic information to control the facile racemization of the optically active selenoxides by incorporating the n_p(Se)−π(Nap), n_p(Se)−π(Ar), and/or n_p(G)- - -σ*(Se−O) interactions suitably into the selenoxides.

Results and Discussion

Structures of 1-[*p*-YC$_6$H$_4$Se(O)]C$_{10}$H$_7$ (1). Single crystals of **1a**, **1b′**,[16] **1d**, **1e**, and **1f** were obtained via slow evaporation of hexane solutions containing dichloromethane, and one of the suitable crystals was subjected to X-ray crystallographic analysis for each compound. Only one type of structure corresponds to each of them in the crystals for **1a**, **1b′**, **1d**, and **1e**, and two types correspond to **1f** in the crystals. Figures 1−3 show the structures of **1a**, **1b′**, and **1e**, respectively. Those of **1d** and **1f** are shown in the Supporting Information.[17] The structures around the Se atoms are essentially the same as those in Figures 1−3, although there are some differences in the torsional angles of C(1)−Se−C(11)−C(12) (= ϕ_{Ar}).

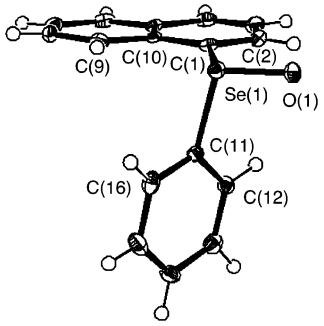

FIGURE 1. Structure of **1a** (thermal ellipsoids are shown at 50% probability levels).

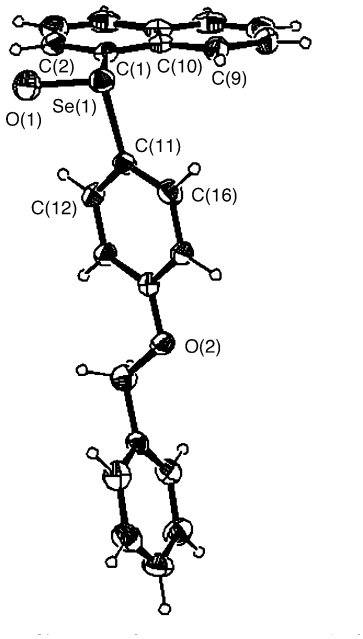

FIGURE 2. Structure of **1b′** (thermal ellipsoids are shown at 40% probability levels).

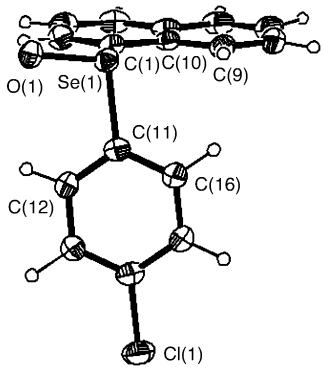

FIGURE 3. Structure of **1e** (thermal ellipsoids are shown at 40% probability levels).

Selected interatomic distances, angles, and torsional angles of **1a**, **1b′**, **1d**, **1e**, and **1f** necessary for the discussion are collected in Table 1. The planarity of the naphthyl (Nap) and

(15) Nakanishi, W.; Hayashi, S.; Shimizu, D.; Hada, M. *Chem. Eur. J.* **2006**, *12*, 3829−3846.

(16) Single crystals of **1b** with Y = OMe were tried to prepare under various conditions. However, single crystals of **1b**, suitable for the X-ray crystallographic analysis, were not obtained. The crystals look amorphous. Instead, single crystals suitable for the X-ray analysis were obtained for **1b′** with Y = $PhCH_2O$. Therefore, the structure of **1b′** is employed in place of **1b** here.

(17) The crystallographic data of **1a**, **1b′**, **1d**, **1e**, **1f**, **2b**, **3c**, **3e**, **4b**, **5**, and **10** are collected in the Supporting Information. The structures of **1d**, **1f**, and **3c** are shown in Figures S1−S3, respectively, in the Supporting Information.

TABLE 1. Selected Bond Lengths, Angles, and Torsional Angles around the Selenium Atom of 1a, 1b′, 1d, 1e, and 1f

	1a	**1b′**	**1d**	**1e**	**1f** (S−A)	**1f** (S−B)
bond lengths (Å)						
Se−C(1)	1.955(3)	1.950(5)	1.963(6)	1.953(3)	1.959(5)	1.960(5)
Se−C(11)	1.945(2)	1.935(4)	1.952(5)	1.959(3)	1.958(4)	1.958(4)
Se−O(1)	1.6630(18)	1.653(3)	1.660(4)	1.665(2)	1.651(4)	1.663(4)
angles (deg)						
Se−C(1)−C(2)	116.2(2)	116.3(4)	115.3(5)	117.0(2)	116.4(4)	114.8(4)
Se−C(1)−C(10)	121.28(19)	121.3(4)	120.9(4)	120.3(2)	121.4(4)	122.8(4)
Se−C(11)−C(12)	120.51(19)	120.7(4)	119.4(4)	118.8(2)	119.1(4)	118.6(4)
C(1)−Se−C(11)	95.41(12)	95.6(2)	94.5(2)	95.9(1)	95.3(2)	94.8(2)
O(1)−Se−C(1)	102.20(10)	102.7(2)	103.2(2)	102.4(1)	101.8(2)	101.2(2)
O(1)−Se−C(11)	103.01(10)	103.3(2)	102.8(2)	101.6(1)	103.9(2)	103.0(2)
torsional angles (deg)						
Se−C(1)−C(2)−C(3)	177.1(2)	−176.6(4)	−174.3(5)	178.0(3)	177.0(4)	−179.1(4)
Se−C(1)−C(10)−C(5)	−174.83(18)	174.9(3)	173.0(4)	−177.9(2)	−175.6(3)	177.5(3)
Se−C(1)−C(10)−C(9)	4.8(4)	−4.7(6)	−6.5(8)	0.9(4)	4.5(7)	0.2(7)
C(1)−Se−C(11)−C(12)	54.6(2)	−53.9(4)	−55.5(5)	−86.5(3)	−71.0(4)	78.1(4)
C(1)−Se−C(11)−C(16)	−131.6(2)	131.5(4)	129.3(5)	95.5(3)	109.5(4)	−103.3(4)
C(2)−C(1)−Se−C(11)	−102.5(2)	104.6(4)	103.8(5)	100.0(3)	97.1(4)	−104.8(4)
C(10)−C(1)−Se−C(11)	75.7(2)	−74.0(4)	−74.8(5)	−82.4(2)	−86.9(4)	76.9(4)
O(1)−Se−C(1)−C(2)	2.1(2)	−0.4(4)	−0.5(5)	−3.3(3)	−8.3(4)	−0.5(4)
O(1)−Se−C(1)−C(10)	−179.7(2)	−179.0(4)	−179.1(4)	174.3(2)	167.7(4)	−178.8(4)
O(1)−Se−C(11)−C(12)	−49.3(2)	50.6(4)	49.1(5)	17.5(3)	32.6(4)	−24.6(4)
type of structure	(**A**: **np**)	(**A**: **np**)	(**A**: **np**)	(**A**: **pd**)	(**A**: **pd**)	(**A**: **pd**)

aryl (Ar) planes is very good. The structures of **1** examined are all **A** for the naphthyl plane. We call this O dependence. Since the structure of **6b** is reported to be (**B**: **pd**),[5b] the O dependence in **1b′** corresponds to the dramatic change in the structure from **6b** (**B**: **pd**) to **1b′** (**A**: **np**), for example.

It is worthwhile to comment on the torsional angles of C(10)−C(1)−Se−C(11) (= ϕ_{Nap}) and C(1)−Se−C(11)−C(12) (= ϕ_{Ar}). A successive change in ϕ_{Ar} is observed depending on Y: (**1x**: ϕ_{Nap}, ϕ_{Ar}) are (**1a**: 75.7(2)°, 54.6(2)°), (**1b′**: −74.0(4)°, −53.9(4)°), (**1d**: −74.8(5)°, −55.5(5)°), (**1e**: −82.4(2)°, −86.5(3)°), (**1f** (S−A): −86.9(4)°, −71.0(4)°), and (**1f** (S−B): 76.9(4)°, 78.1(4)°) (Table 1). While the structure around the Nap group in **1** is all **A**, the conformation around the Ar group changes almost successively depending on Y. We call the structural change Y dependence. The observed results are explained by assuming that the structure is **pd** when Y is accepting and it changes **np** if Y goes to donating. The strong accepting nitro group in **1f** and the chloro group in **1e** control the structures **pd**. They are denoted by (**A**: **pd**) (cf. Scheme 1). The structures of **1a**, **1b′**, and **1d** are (**A**: **np**). Typical (**A**: **pl**) is not observed.

Structures of 8-G-1-[*p*-YC$_6$H$_4$Se(O)]C$_{10}$H$_6$ (2−4). Similarly to the case of **1**, structures of **2b**, **3c**, **3e**, and **4b** were determined by the X-ray crystallographic analysis. Only one type of structure corresponds to each of them in the crystals. Figures 4−6 exhibit the structures of **2b**, **3e**, and **4b**, respectively. The structure of **3c** is shown in the Supporting Information[17] and is essentially the same as that in Figures 4−6.

Selected interatomic distances, angles, and torsional angles of **2b**, **3c**, **3e**, and **4b** necessary for the discussion are shown in Table 2. The planarity of the naphthyl and aryl planes in **2**−**4** is good. Each Se−O bond is on the naphthyl plane as observed in **1**. Consequently, three G- - -Se−O (G = F, Cl, and Br) atoms in **2**−**4** align linearly. We call this G dependence. The structures containing the linear alignment of the three G- - -Se−O atoms in **2**−**4** must be stabilized by the hypervalent G- - -Se−O 3c−4e interactions, in addition to the O dependence, which is also operating in **1**. The O and G atoms in **3** and **4** deviate from the Nap plane to some extent. The O, Y, and G dependences are summarized in Scheme 2. Torsional angles of C(1)−Se−C(11)−C(12) in **2**−**4** are close to 90°. The structures

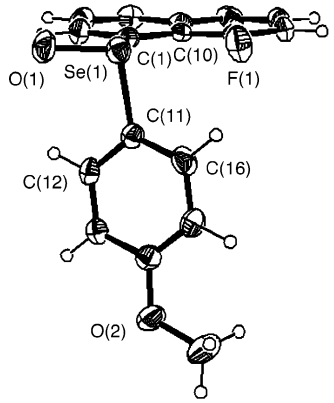

FIGURE 4. Structure of **2b** (thermal ellipsoids are shown at 40% probability levels).

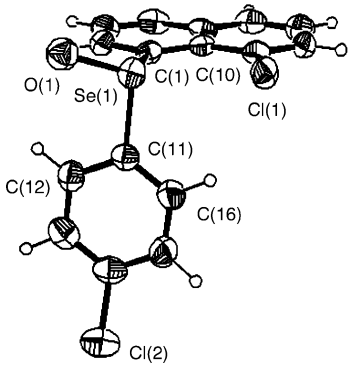

FIGURE 5. Structure of **3e** (thermal ellipsoids are shown at 40% probability levels).

of **2b**, **3c**, **3e**, and **4b** are (**A**: **pd**). It is difficult to recognize the Y dependence in the structures of **2**−**4**.

Structures of (1-C$_{10}$H$_7$)$_2$Se=O (5) and (1-C$_{10}$H$_7$)$_2$Se (10). The structures of **5** and 1,1′-dinaphthyl selenide (**10**) were determined similarly. Only one type of structure corresponds to each of them in the crystals. Figures 7 and 8 show the structures of **5** and **10**, respectively.

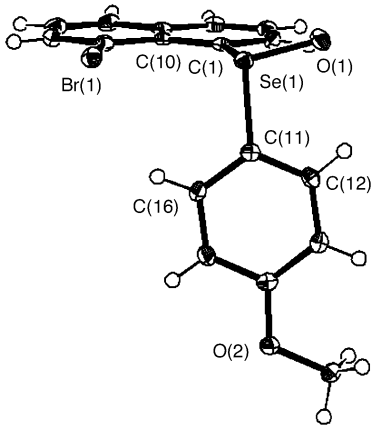

FIGURE 6. Structure of **4b** (thermal ellipsoids are shown at 50% probability levels).

TABLE 2. Selected Bond Lengths, Angles, and Torsional Angles around the Selenium Atom of 2b, 3c, 3e, and 4b

	2b	3c	3e	4b
bond lengths (Å)				
Se−C(1)	1.965(3)	1.985(4)	1.989(7)	1.986(3)
Se−C(11)	1.944(3)	1.966(4)	1.976(7)	1.961(3)
Se−G	2.807(2)	3.069(1)	3.067(2)	3.191(3)
Se−O(1)	1.664(2)	1.658(3)	1.658(6)	1.661(2)
angles (deg)				
Se−C(1)−C(2)	115.3(2)	110.8(4)	111.6(6)	111.6(2)
Se−C(1)−C(10)	123.5(2)	127.1(3)	126.7(5)	127.2(2)
Se−C(11)−C(12)	118.9(2)	117.9(3)	115.9(6)	117.0(2)
C(1)−Se−C(11)	96.6(1)	95.9(2)	94.5(3)	94.16(11)
O(1)−Se−C(1)	100.7(1)	100.4(2)	101.1(3)	101.39(11)
O(1)−Se−C(11)	102.0(1)	100.6(1)	101.2(3)	100.98(11)
C(1)−Se−G	71.28(9)	74.5(1)	75.4(2)	71.02
O(1)−Se−G	170.85(8)	171.2(1)	164.6(2)	163.58
torsional angles (deg)				
Se−C(1)−C(2)−C(3)	177.8(2)	−177.1(4)	178.3(6)	179.9(2)
Se−C(1)−C(10)−C(5)	−178.4(2)	175.4(3)	−177.0(5)	−179.86(19)
Se−C(1)−C(10)−C(9)	0.8(4)	−5.3(6)	2(1)	−0.5(4)
C(1)−Se−C(11)−C(12)	−72.6(2)	−70.8(4)	−90.3(6)	105.1(2)
C(1)−Se−C(11)−C(16)	110.2(3)	116.2(4)	93.1(7)	−77.1(2)
C(2)−C(1)−Se−C(11)	102.2(2)	99.7(3)	88.3(5)	−85.5(2)
C(10)−C(1)−Se−C(11)	−81.3(2)	−79.0(3)	−94.8(6)	94.6(2)
O(1)−Se−C(1)−C(2)	−1.3(2)	−2.2(3)	−14.1(6)	16.5(2)
O(1)−Se−C(1)−C(10)	175.1(2)	179.1(3)	162.9(6)	−163.3(2)
O(1)−Se−C(11)−C(12)	29.9(2)	30.9(4)	11.9(6)	2.7(2)
G−C(9)−C(10)−C(5)	178.3(2)	176.0(3)	178.6(5)	−179.56(19)
type of structure	(**A**: **pd**)	(**A**: **pd**)	(**A**: **pd**)	(**A**: **pd**)

Selected data of **5** and **10** necessary for the discussion are shown in Table 3. The structure of **5** is **A** for both naphthyl groups (**5** (**AA**)), and the planarity of the naphthyl planes is very good. It constructs a roof structure. On the other hand, the structure of **10** is **AB** (Figure 8). **10** (**AB**) changes dramatically to **5** (**AA**) by the O dependence. **5** (**AA**) provides a hint for the mechanism of the Y dependence in **1**.

Why are such structures observed in **1**−**5**? The origin of the O, Y, and G dependences is analyzed on the basis of the quantum chemical (QC) calculations.

QC Calculations. QC calculations were performed on 1-(methylseleninyl)naphthalene (**11**) and the derivatives bearing G of halogens at the 8-positions [**12** (G = F), **13** (G = Cl), and **14** (G = Br)] to elucidate the origin of the O and G dependences (Chart 2). Indeed, the structures and the energies evaluated on the basis of the QC calculations essentially correspond to those in the gas phase, but the factors to control and/or stabilize the structures in the gas phase must also operate in solid states and in solutions. However, we must be careful since other factors,

SCHEME 2. O, Y, and G Dependence in 8-G-1-[*p*-YC$_6$H$_4$Se(O)]C$_{10}$H$_6$ (Y and G Dependence in 8-G-1-(*p*-YC$_6$H$_4$Se)C$_{10}$H$_6$ in Parentheses)

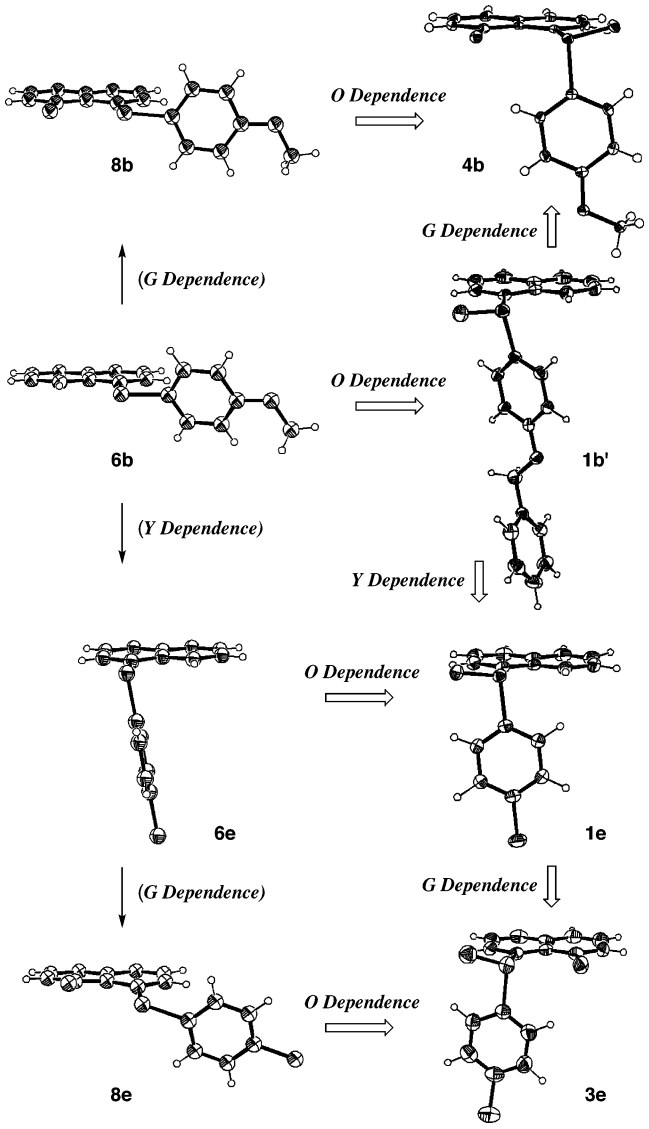

such as the crystal packing effect in crystals and the solvent effect in solutions, would be stronger than those predicted by QC calculations.[18] Selenoxides **11**−**14** are mainly discussed, instead of **1**−**4**, to elucidate observed structures around the Nap group, first. Those around the Ar group are also discussed on the basis of the optimized structure of **1a**.

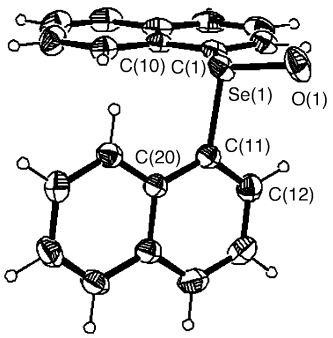

FIGURE 7. Structure of **5** (thermal ellipsoids are shown at 40% probability levels).

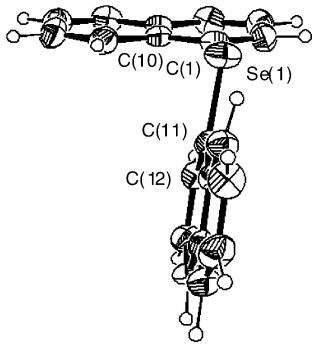

FIGURE 8. Structure of **10** (thermal ellipsoids are shown at 40% probability levels).

TABLE 3. Selected Bond Lengths, Angles, and Torsional Angles around the Selenium Atom of 5 and 10

	5	10
bond lengths (Å)		
Se−C(1)	1.955(3)	1.911(4)
Se−C(11)	1.963(3)	1.910(4)
Se−O(1)	1.653(3)	
angles (deg)		
Se−C(1)−C(2)	117.3(3)	123.5(4)
Se−C(1)−C(10)	120.0(3)	117.3(3)
Se−C(11)−C(12)	117.7(3)	118.9(4)
C(1)−Se−C(11)	96.0(1)	99.9(2)
O(1)−Se−C(1)	102.0(1)	
O(1)−Se−C(11)	101.8(1)	
torsional angles (deg)		
Se−C(1)−C(2)−C(3)	−177.3(3)	177.8(4)
Se−C(1)−C(10)−C(5)	176.2(2)	−177.6(3)
Se−C(1)−C(10)−C(9)	−3.2(4)	2.5(6)
C(1)−Se−C(11)−C(12)	64.0(3)	−102.1(4)
C(1)−Se−C(11)−C(20)	−117.2(3)	80.2(4)
C(2)−C(1)−Se−C(11)	−101.2(3)	−0.1(5)
C(10)−C(1)−Se−C(11)	83.5(3)	178.4(3)
O(1)−Se−C(1)−C(2)	2.2(3)	
O(1)−Se−C(1)−C(10)	−173.1(2)	
O(1)−Se−C(11)−C(12)	−39.6(3)	
type of structure	**AA**	**AB**

CHART 2

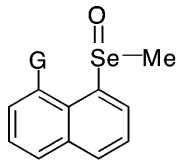

11 (G = H), **12** (G = F)
13 (G = Cl), **14** (G = Br)

The B3LYP/6-311+G(d) method of the Gaussian 98 program[19] is employed in the calculations of **11**−**14**.[20] Two stable structures and two transition states are optimized for **11**−**13** and three minima and three transition states are for **14**. Frequency analysis is performed on the six optimized structures of **14** with the B3LYP/6-311+G(d)//B3LYP/6-311+G(d) method. All frequencies are predicted to be positive for the three minima, and only one negative (imaginary) frequency is for each of the transition state. Consequently, the nature of the optimized structures is demonstrated to be as expected. Table 4 shows the results.[21] The relative energies for the structures do not change so much by the thermal effects.

The B3LYP/6-311+G(2d,p) method is also applied to optimize further the two stable structures and the two transition states of **11** and the three stable conformers of **14**. The results are also collected in Table 4. The relative energies obtained with the B3LYP/6-311+G(d) method are essentially the same as those with the B3LYP/6-311+G(2d,p) method. QC calculations are also performed on **1a** and the protonated global minimum of **11** (**11A**•H^+) with the B3LYP/6-311+G(2d,p) method.

Energy Profile of 8-G-1-[MeSe(O)]$C_{10}H_6$ (11−14). To clarify the energy profile of naphthyl selenoxides, **11** are further optimized with variously fixed torsional angles ϕ_{Me} (= $\angle C_9C_1SeC_{Me}$) by the B3LYP/6-311+G(2d,p) method. The energies of **11** are plotted versus ϕ_{Me}, together with those of fully optimized energies in Table 4 calculated with the same method. Figure 9 shows the plot. The four (full) optimized structures are on the energy surface: two must be minima and two are the transition states, as expected. The nature of the optimized structures for **12** and **13** is also assumed to be that expected, since the calculation method for **12** and **13** is the same as that for **11** and **14**.

The global minima of **11**−**14** are shown by **11A**−**14A**, respectively, which reproduce the observed structures around the naphthyl seleninyl moieties of **1**−**4**, respectively. The stable structures of **14** are called **14A**, **14B**, and **14C**, of which ϕ_{Me} are 80.5°, 192.6°, and 303.4°, respectively, where the B3LYP/6-311+G(d) method is employed for the calculations. The transition states are **14** (TS, **AB**), **14** (TS, **BC**), and **14** (TS, **CA**), of which ϕ_{Me} are 178.8°, 265.1°, and 330.9°, respectively, where **14** (TS, **AB**) is a transition state between **14A** and **14B**, for example. Table 4 collects the relative energies (ΔE) of the optimized structures for **11**−**14**, where the energies of **11A**−**14A** are taken to be the standards, respectively. The optimized values for ϕ_{Me}, together with ϕ_O (= $\angle C_9C_1SeO$), are also collected in Table 4. Scheme 3 shows the stable structures and the transition states optimized for **14**, for example. If one examines ϕ_{Me} in Table 4, one will easily realize that the stable conformers **11B**, **12B**, and **13B** are not optimized. Namely, stable conformers other than **11A**−**13A** in **11**−**13** are **11C**−**13C**, respectively. While the structure of the transition state between **11A** and **11C** corresponds to that of **14** (TS, **AB**), those for **12** and **13** are similar to that of **14** (TS, **BC**) (Table 4). Therefore, the transition state of **11** between **11A** and **11C** is assigned to **11** (TS, **AB**) and those for **12** and **13** are **12** (TS, **BC**) and **13** (TS, **BC**), respectively.

(18) The structures of **1** in chloroform solutions are also determined employing δ(H) at the 2- and 8-positions. The results are the same as those obtained from the X-ray crystallographic analysis. The structures of **2**−**4** are determined similarly in solutions. The results will be reported elsewhere.

(19) *Gaussian 98* (Revision A.11): Frisch, M. J.; Trucks, G. W.; Schlegel, H. B.; Scuseria, G. E.; Robb, M. A.; Cheeseman, J. R.; Zakrzewski, V. G.; Montgomery, J. A.; Stratmann, Jr., R. E.; Burant, J. C.; Dapprich, S.; Millam, J. M.; Daniels, A. D.; Kudin, K. N.; Strain, M. C.; Farkas, O.; Tomasi, J.; Barone, V.; Cossi, M.; Cammi, R.; Mennucci, B.; Pomelli, C.; Adamo, C.; Clifford, S.; Ochterski, J.; Petersson, G. A.; Ayala, P. Y.; Cui, Q.; Morokuma, K.; Salvador, P.; Dannenberg, J. J.; Malick, D. K.; Rabuck, A. D.; Raghavachari, K.; Foresman, J. B.; Cioslowski, J.; Ortiz, J. V.; Baboul, A. G.; Stefanov, B. B.; Liu, G.; Liashenko, A.; Piskorz, P.; Komaromi, I.; Gomperts, R.; Martin, R. L.; Fox, D. J.; Keith, T.; Al-Laham, M. A.; Peng, C. Y.; Nanayakkara, A.; Challacombe, M.; Gill, P. M. W.; Johnson, B.; Chen, W.; Wong, M. W.; Andres, J. L.; Gonzalez, C.; Head-Gordon, M.; Replogle, E. S.; Pople, J. A. Gaussian, Inc., Pittsburgh, PA, 2001.

(20) In our experience, the 6-311+G(d) basis sets or higher ones are recommended, when usual organic selenium compounds are calculated. See, for example, refs 4h, 5b, and: Nakanishi, W.; Hayashi, S. *J. Phys. Chem.* A **1999**, *103*, 6074−6081.

(21) The carbons are numbered equal to those in the names, which are not the same as those in the structures determined by the X-ray analysis.

TABLE 4. Calculated Energies and Torsional Angles (ϕ_{Me} and ϕ_O) for 11−14, Together with the Results of Frequency Analysis for 14

	A	TS: **AB**	**B**	TS: **BC**	**C**	TS: **CA**
			With the B3LYP/6-311+G(d) Method			
E(**11**) (au)	−2902.0304	−2902.0221	*a*	*a*	−2902.0277	−2902.0137
ΔE^b(kJ mol^{-1})	0.0	21.8			7.1	43.8
$\phi_{Me}{}^c$ (deg)	80.7	166.4			284.6	360.4
$\phi_O{}^d$ (deg)	185.5	273.1			30.7	108.0
E(**12**) (au)	−3001.3000	*a*	*a*	−3001.2786	−3001.2872	−3001.2766
ΔE^b(kJ mol^{-1})	0.0			56.1	33.6	61.4
$\phi_{Me}{}^c$ (deg)	79.5			242.5	291.2	366.7
$\phi_O{}^d$ (deg)	183.5			344.9	41.3	101.4
E(**13**) (au)	−3361.6478	*a*	*a*	−3361.6250	−3361.6320	−3361.6183
ΔE^b(kJ mol^{-1})	0.0			59.9	41.5	77.5
$\phi_{Me}{}^c$ (deg)	80.5			254.7	298.4	327.6
$\phi_O{}^d$ (deg)	183.5			356.4	49.1	74.3
E(**14**) (au)	−5475.5651	−5475.5502	−5475.5503	−5475.5423	−5475.5484	−5475.5331
ΔE^b(kJ mol^{-1})	0.0	39.1	38.9	59.9	43.8	84.0
$\phi_{Me}{}^c$ (deg)	80.5	178.8	192.6	265.1	303.4	330.9
$\phi_O{}^d$ (deg)	183.3	283.2	296.2	352.9	54.3	141.0
$\nu_1{}^{e,f}$ (cm^{-1})	31.7	−24.8	21.2	−42.1	25.2	−65.6
$\nu_2{}^{e,g}$(cm^{-1})	87.8	37.2	52.7	35.3	73.6	39.9
ZPC^{e,h} (au)	0.1667	0.1662	0.1664	0.1659	0.1663	0.1662
TCF^{e,i} (au)	0.1252	0.1262	0.1245	0.1254	0.1244	0.1261
$E_F{}^{e,j}$ (au)	−5475.4399	−5475.4240	−5475.4259	−5475.4169	−5475.4240	−5475.4070
$\Delta E_F{}^{e,k}$ (kJ mol^{-1})	0.0	41.7	36.8	60.4	41.7	86.4
meaning	minimum	saddle point	minimum	saddle point	minimum	saddle point
			With the B3LYP/6-311+G(2d,p) Method			
E(**11**) (au)	−2902.0639	−2902.0558	*a*	*a*	−2902.0614	−2902.0474
ΔE^b(kJ mol^{-1})	0.0	21.3			6.6	43.3
$\phi_{Me}{}^c$ (deg)	80.8	165.8			284.5	359.9
$\phi_{Me}{}^d$ (deg)	185.6	272.5			30.7	108.0
E(**14**) (au)	−5475.5935	*l*	−5475.5790	*l*	−5475.5767	*l*
ΔE^b(kJ mol^{-1})	0.0		38.1		44.1	
$\phi_{Me}{}^c$ (deg)	−80.8		192.8		301.8	
$\phi_O{}^d$ (deg)	183.5		296.5		52.9	

[a] Not optimized. [b] $\Delta E = E(\mathbf{X}) - E(\mathbf{A})$, where X = A, B, C, AB, BC, and/or CA for each. [c] $\phi_{Me} = \angle C_9C_1SeC_{Me}$.[21] [d] $\phi_O = \angle C_9C_1SeO$.[21] [e] Frequency analysis carried out with the B3LYP/6-311+G(d)//B3LYP/6-311+G(d) method. [f] Lowest frequency obtained by the frequency analysis. [g] Second lowest frequency obtained by the frequency analysis. [h] Zero-point correction. [i] Thermal correction to Gibbs free energy at 298.15 K. [j] Sum of electronic and thermal Gibbs free energies at 298.15 K. [k] $\Delta E_F = E_F(\mathbf{X}) - E_F(\mathbf{A})$, where X = A, B, C, AB, BC, and CA. [l] Not calculated.

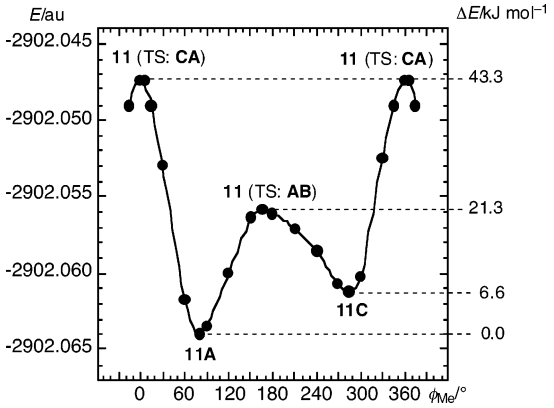

FIGURE 9. Energy profile of **11**.

The Se−O bond is on the naphthyl plane in the global minimum of **11A**, where $\phi_{Me} = 80.8°$ and $\phi_O = 185.6°$. The H-8 atom in **11C** is surrounded by the O, Se, and C_{Me} atoms, which can be derived from **14C** in Scheme 3. The steric repulsion between H-8 and the O−Se−C_{Me} energy wall must be responsible for **11C** being less stable than **11A**. The optimized transition state between **11C** and **11A** is **11** (TS: **CA**). The other local minimum, **11B**, corresponding to **14B**, is searched for. However, **11B** is not optimized. Instead, a somewhat complex energy surface was observed in this region as shown in Figure 9, which exhibit a complex energy profile near the region.

SCHEME 3. Optimized Structures in 14: 14A, 14B, 14C, 14 (TS: AB), 14 (TS: BC), and 14 (TS: CA)

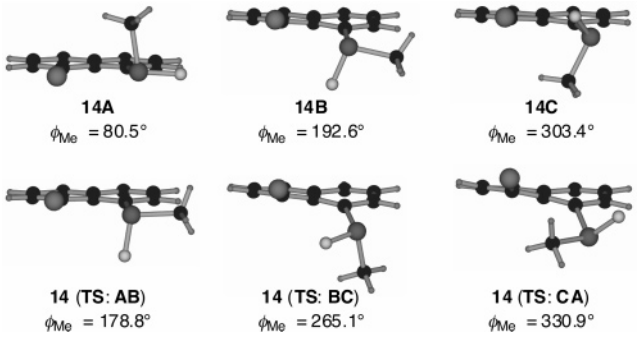

The relative energies of **11A**, **11C**, **11** (TS: **AB**), and **11** (TS: **CA**) are 0.0, 6.6, 21.3, and 43.3 kJ mol^{-1}, respectively. **11** (TS: **CA**) is most unstable, where the Me group is just passing through H-8. It is puzzling why **11** (TS: **BC**) is not optimized, where the O atom is passing through H-8. We propose a mechanism that consists of two factors. One is the steric repulsion between H-8 and O, which must generate **11** (TS: **BC**) (and **11B**). Another factor is an attractive one, which lays the Se−O bond on the naphthyl plane. The latter factor must also operate in **11A**. The origin of the factor will be discussed later. The contribution of the attractive factor may be stronger than the repulsive one in the region since **11** (TS: **BC**) (and **11B**) does not appear in the energy surface of **11**.

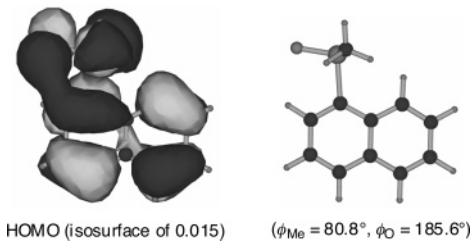

FIGURE 10. HOMO of **11A**, together with the optimized structure.

Origin of O and Y Dependences in 1. What is the origin of the O dependence in **1**? The Se−O bonds are on the naphthyl planes in the observed structures of **1** [ϕ_O(O(1)−Se−C(1)−C(10)) ≈ 180°]. It is instructive to examine the orbital interactions between π(Nap) and the orbitals of the ArSe(O) group.

Two types of interactions must be of importance if the structures of **1** are considered. One is the interaction of π(Nap) with σ*(Se−C) and π*(Nap) with σ(Se−C). Since both π(Se═O) and π*(Se═O) are filled with electrons, the other one must be that of π*(Nap) with π(Se═O) and π*(Se═O). The Se−C_{Ar} bond becomes perpendicular to the naphthyl plane if the π(Nap)−σ*(Se−C_{Ar}) and π*(Nap)−σ(Se−C_{Ar}) interactions are predominant. On the other hand, the Se−O bond will be on the naphthyl plane when the π*(Nap)−π(Se═O) and π*(Nap)−π*(Se═O) interactions substantially contribute to **1**. Observed torsional angles of C(10)C(1)SeC(11) in **1a**, **1b′**, and **1d** are 74.0−75.7°, whereas the corresponding angles of O(1)−Se−C(1)−C(10) are 179.0−179.7° (Table 1). The former deviate ca. 15° from 90° but the latter are very close to 180°. The observations support the mechanism of the π*(Nap)−π(Se═O) and π*(Nap)−π*(Se═O) interactions.[22]

Let us consider the mechanism with the π*(Nap)−π(Se═O) and π*(Nap)−π*(Se═O) interactions in more detail. Since both π(Se═O) and π*(Se═O) are filled with electrons as mentioned above and Se is three coordinated, both π(Se═O) and π*(Se═O) must localize on O. They are reduced to an n_p(O), in this case. Consequently, there are two n_p(O)'s, since O has the original one. To clarify the discussion, two n_p(O)'s are used in the discussion here. The two n_p(O)'s are n_{py}(O) and n_{pz}(O), perpendicular with each other, if the direction of the Se−O bond is fixed at the *x*-axis and that of the p orbitals of π(Nap) in **1**−**4** is fixed at the *z*-axis (π_z(Nap)). Since O in Se^+═O^- is highly negatively charged and π*(Nap) must act as a good acceptor, CT will occur mainly directly from n_p(O) to π*(Nap). The mechanism must be essentially the same as the through-space one.

Figure 10 shows HOMO of **11A**,[23] which demonstrates the overlap between the nonbonded n_p(O) and π*(Nap) orbitals in **11A**.[24] The O dependence in **1** is well understood and explained by the nonbonded n_p(O)- - -π(Nap) interaction. The mechanism must also be operating in **2**−**4**.

In the case of **5** (**AA**), it contains two π(Nap)'s, perpendicular with each other. If the directions of the π(Nap)'s are set to the *y*- and *z*-axes (π_y(Nap_B) and π_z(Nap_A), respectively) with the Se−O bond to the *x*-axis, two n_p(O)'s are called n_{pz}(O) and n_{py}(O), which are perpendicular with each other. Consequently, n_{pz}(O) interacts with π_z(Nap_A) and n_{py}(O) does with π_y(Nap_B)

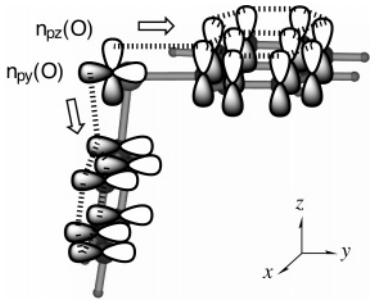

FIGURE 11. Proposed nonbonded n_{pz}(O)- - -π(Nap) and n_{py}(O)- - -π(Ar) interactions in **1** (**A**: **pd**), together with the direction of CT. Optimized structure of **1a** (**A**: **pd**) is employed as the framework.

in **5** (**AA**). The structure of **5** (**AA**) is well explained by the O dependence of the two nonbonded n_p(O)- - -π(Nap) interactions. Namely, the double but independent n_p(O)- - -π(Nap) interactions occur in **5**, which determine the **AA** structure. This idea leads to the mechanism of the Y dependence in **1**.

If the accepting ability of π(Ar) in NapSe(O)Ar is not less than that of π(Nap), the conformation around the Ar group in **1** must be very close to that of a Nap group in **5** (**AA**). It requires Y of accepting groups, which explains well the structures of **1** (**A**: **pd**) with Y = Cl and NO_2.[25,26] The discussion is summarized in Figure 11. The structure will be no longer **1** (**A**: **pd**) if the accepting ability of π(Ar) becomes less than that of π(Nap). The **1** (**A**: **pd**) structure changes to **1** (**A**: **np**) as observed in **1** with Y = H, Me, and OCH_2Ph. The **1** (**A**: **pl**) structure is not observed since the n_{py}(O)- - -π(Ar) interaction must be repulsive for Ar with Y of donating groups.

QC calculations were performed on **1a** with the B3LYP/6-311+G(2d,p) method. The **1a** (**A**: **pd**) structure is optimized with ϕ_{Nap} = 89.5° and ϕ_{Ar} = 103.7° (and −79.4°). The same structure was optimized even if the calculations started from **1a** (**A**: **pl**) and **1a** (**B**: **pd**). The optimized structure of **1a** (**A**: **pd**) with ϕ_{Ar} = −79.4° did not reproduce the observed **1a** (**A**: **np**) of ϕ_{Ar} = 54.6(2)°. Instead, the calculations demonstrates the importance of the nonbonded n_p(O)- - -π(Ph) interaction (O dependence for Ph) since the torsional angle of $OSeC_iC_o$ is predicted to be −0.7° (and 176.2°). The optimized structure is employed as the framework of **1a** (**A**: **pd**) in Figure 11.

Why does the nonbonded n_p(O)- - -π(Nap) interaction control the structure of **1** so effectively? The observed *r*(O, C(1)) and *r*(O, C(2)) values in **1** are collected in Table 5. They are 2.806−2.845 and 2.880−2.960 Å, respectively, which are 0.38−0.41

(22) The values for **1e** and **1f** (averaged of **1f** (S−A) and **1f** (S−B)) are different from those shown above, of which deviations are 6−7°. It may be due to the pure (**A**: **pd**) structures for **1e** and **1f**. Similar deviations are observed in **5** (**AA**), where both π(Nap) interact with π(Se═O), identically.

(23) *MolStudio R3.2* (Rev 1.0), NEC Corp., 1977−2003.

(24) Natural charges (*Qn*) are calculated for a naphthalene adduct of NapH- - -M. For M of O═$SeMe_2$, the O−Se−^{A}C atoms in NapH- - -O═Se^AMeMe are placed in the NapH plane with *r*(O, C_1) and *r*(O, C_2) being fixed at 2.822 and 2.936 Å, respectively (cf: Table 5). *Qn*($OSeMe_2$) in NapH- - -$OSeMe_2$ is calculated to be 0.0075, which means that CT from $OSeMe_2$ to NapH in the adduct is −0.0075. CT of ca. 1% from Me_2SeO to NapH in NapH- - -$OSeMe_2$ seems reasonable in such adduct. Since Nap in **1**−**4** are substituted with the highly positively charged $ArSe^+$(═O^-) group, CT from O to Nap in **1**−**4** must be larger than that calculated for NapH- - -$OSeMe_2$. In the case of NapH- - -M with M = O^{2-}, MeO^-, and $MeSeO^-$, CT from M to NapH are evaluated to be −0.750, −0.046, and −0.030, respectively.

(25) A good correlation between EA and ϵ(LUMO) at the DFT level is suggested: *Chemical Hardness*; Pearson, R. G., Ed.; Wiley-VCH: New York, 1997; p 38.

(26) EA of anisole, benzene, chlorobenzene, nitrobenzene are reported to be −1.11, −1.15, −0.75, and 1.01 eV, respectively.[36] EA of naphthalene is estimated to be −0.185 eV, based on its ϵ (LUMO) calculated by the B3LYP/6-311+G(d,p) method.[23,5b]

TABLE 5. Observed Nonbonded O(1)- -C(1) and O(1)- -C(2) Distances of 1−4

compd	1a	1b′	1d	1e	1f (S−A)	1f (S−B)	2b	3c	3e	4b
O(1)- - -C(1) (Å)	2.822(2)	2.820(6)	2.845(7)	2.826(4)	2.809(6)	2.806(6)	2.801(3)	2.809(5)	2.823(9)	2.829(3)
O(1)- - -C(2) (Å)	2.936(2)	2.942(7)	2.951(9)	2.960(4)	2.938(6)	2.880(8)	2.884(4)	2.796(6)	2.851(10)	2.870(2)

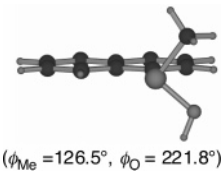

FIGURE 12. Optimized structure of **11A**•H^+ (ϕ_{Me} = 126.5° and ϕ_O = 221.8°) with the B3LYP/6-311+G(2d,p) method.

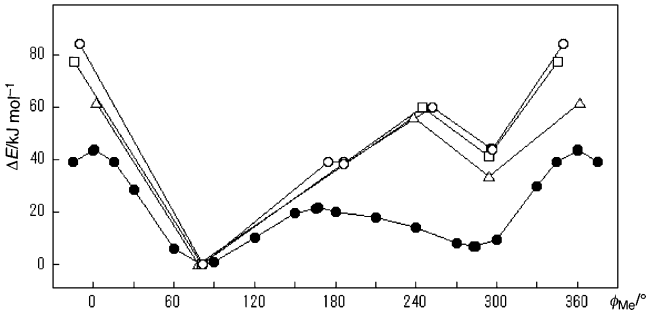

FIGURE 13. Energy profiles for **11** (●), **12** (△), **13** (□), and **14** (○) calculated with the B3LYP/6-311+G(d) method, together with that of **11** (●) with the B3LYP/6-311+G(2d,p) method.

and 0.26−0.34 Å shorter than the sum of van der Waals radii of O and C atoms, respectively (r_{vdW}(C) = 1.70 Å and r_{vdW}(O) = 1.52 Å: Σr_{vdW} =3.22 Å).[27] The orbital interaction must work more effective to control the structures of **1** than that expected based on r_{vdW}(O), since n_p(O) in **1** extends further in space than that estimated from r_{vdW}(O), with O of highly negatively charged.

The contribution of the n_{pz}(O)- - -π(Nap) interaction in **11** is also demonstrated by comparing the optimized structure of **11A** with that of **11A′** where the n_{pz}(O) is removed. **11A′** is actualized by protonating **11A** at the n_{pz}(O) (**11A**•H^+). **11A**•H^+ is optimized with the B3LYP/6-311+G(2d,p) method. Figure 12 shows the optimized structure of **11A**•H^+. If the calculations are started with an initial structure around the Se═O moiety close to that of **11A**, it is optimized to be that shown in Figure 12. The optimized **11A**•H^+ is essentially the same as the initial one, except for the torsional angles of ϕ_{Me} and ϕ_O. The Se−O bond in **11A**•H^+ rotates around Se−C_{Nap}, relative to that in **11A**, to give ϕ_{Me} = 126.5° and ϕ_O = 221.8°. This must be the results of the disappearance of n_{pz}(O) in **11A**•H^+. The results supports the importance of the n_{pz}(O)- - -π(Nap) interaction in **11A**, together with that in **1**.

Effects of G in 8-G-1-[MeSe(O)]$C_{10}H_6$ (11−14). Effects of G of halogens at the 8-positions in **12**−**14** are examined next. Figure 13 shows the plots of energies of **12**−**14** versus ϕ_{Me} shown in Table 4, together with those of **11** shown in Figure 9, for convenience of comparison. The repulsive and attractive interactions caused by G of halogens in **12**−**14**, relative to G = H in **11**, are clarified and visualized in Figure 13.

Two stable structures and two transition states are optimized for **11**−**13** and three minima and three transition states are for **14**, as discussed in the previous sections (Table 4). The global minima of **11**−**14** are **11A**−**14A**, respectively. Although **11A** is stabilized only by the O dependence (the n_p(O)- - -π(Nap) interaction), **12A**−**14A** are stabilized both by the O and G dependences (the n_p(O)- - -π(Nap) and n_p(G)- - -σ*(Se−O) 3c−4e interactions, respectively). The contribution of the O dependence in **11** could be roughly estimated by the energy difference between **11** (TS, **AB**) and **11A**, which is 22 kJ mol^{-1}, if calculated with the B3LYP/6-311+G(d) method. The difference between **14** (TS, **AB**) and **14A** is 39 kJ mol^{-1}. The value contains the O dependence, the G dependence, and the steric repulsion between Br and Se. If the O dependence in **14** is assumed to be equal to that in **11**, the sum of the G dependence and the steric repulsion between Br and Se in **14** is estimated to be 17 kJ mol^{-1} (= 39−22 kJ mol^{-1}). The results show that contributions of the O and G dependences are close with each other in **14**, if the steric repulsion is contained in the G dependence. Both values are around 20 kJ mol^{-1}.

The n_p(Br)- - -σ*(Se−C) interaction must play an important role in **14B**.[4h] However, it is difficult to estimate the contribution of the n_p(Br)- - -σ*(Se−C) interaction since it works behind other factors of larger contributions. Although **12B** and **13B** are not optimized as local minima, the n_p(G)- - -σ*(Se−C) (G = F and Cl) interactions must also operate in **12** and **13**.[28] They would be too small to give the local minima in **12** and **13**.

The ΔE values of **n** (TS: **CA**) (n = 11−14) are 44,[29] 61, 78, and 84 kJ mol^{-1}, respectively, which correspond to the steric repulsive energies between Me and G of H, F, Cl, and Br, respectively (Table 4). The contribution of the steric factor in the naphthalene 1,8-positions is confirmed to be an order of G = H ≪ F ≪ Cl < Br based on the values. A similar trend is also predicted in **n** (**C**) (n = 11−14). The ΔE values are 7, 33, 42, and 44 kJ mol^{-1}, respectively, which exhibit the magnitudes of the steric repulsion between the O−Se−C_{Me} energy wall and G of H, F, Cl, and Br, respectively.

On the other hand, almost equal ΔE values are obtained for **n** (TS: **BC**) (n = 12−14). They are 56, 60, and 60 kJ mol^{-1}, respectively, which correspond to the steric repulsion between the O atom and G of F, Cl, and Br, respectively. Some energy-lowering mechanisms, other than the steric repulsion, would operate for the heavier atoms, especially for Br, in the transition states. The energy-lowering mechanisms would contain the attractive interactions between the nonbonded atoms and/or the relief of the severe steric repulsion by the easier deformation of the bond angles in the heavier atoms. In the case of **11**, the steric repulsion between O and G of H does not give a transition state of the **11** (TS: **BC**) type. The O dependence must play an important role in the disappearance of **11** (TS: **BC**).

(27) Bondi, A. *J. Phys. Chem.* **1964**, *68*, 441−451.

(28) Contributions of the n_p(G)- - -σ*(Se−C) interactions are evaluated to be approximately 11 kJ mol^{-1} for **7a**−**9a**.[4h]

(29) While the energy difference between **11** (TS: **CA**) and **11A** (ΔE (**11**) = E (**11** (TS: **CA**))−E (**11A**)) is 43 kJ mol^{-1}, that in **15** (1-MeSeNap) (ΔE (**15**)) is 26 kJ mol^{-1}, if calculated with the B3LYP/6-311+G(2d,p) method.[37] Since the difference in **15** does not contain the O dependence, the $\Delta\Delta E$ value [= ΔE(**11**) − ΔE(**15**)] of 17 kJ mol^{-1} should corresponds to the contribution of the O dependence in **11**. The value is close to that estimated in the text.

Factors to determine the structures of naphthyl selenoxides are well established by the experimental investigations on **1**−**5** and based on theoretical calculations mainly on **11**−**14**.

Conclusion

Factors to determine the structures of 8-G-1-[*p*-YC_6H_4Se-(O)]$C_{10}H_6$ [**1** (G = H), **2** (G = F), **3** (G = Cl), and **4** (G = Br)] and $(1\text{-}C_{10}H_7)_2Se{=}O$ (**5**) are clarified, which are called O, G, and Y dependences. The structures of **1**−**4** are all **A** and that of **5** is **AA**, with regard to the Nap group. The factor is the O dependence. The origin is the nonbonded $n_p(O)$- - -π(Nap) interaction operating in **1**−**5**. The $n_p(O)$- - -π(Nap) interaction lays the Se−O bond on the naphthyl plane, which explains the observed structures. **1** (**A**) is stabilyzed by the $n_p(O)$- - -π(Nap) interaction and **5** (**AA**) is the results of the double $n_{pz}(O)$- - -$\pi_z(Nap_A)$ and $n_{py}(O)$- - -$\pi_y(Nap_B)$ interactions, which are independent and perpendicular with each other. If the accepting ability of π(Ar) is not less than that of π(Nap), the structures of **1** around the Se−O bonds are very close to that in **5** (**AA**), namely, they are **1** (**A**: **pd**). In this case, Y of the accepting groups, such as Cl or NO_2, is required. If π(Ar) in **1** is rather donating, the structure changes to **1** (**A**: **np**) (Y dependence). The G dependence is the nonbonded $n_p(G)$- - -σ^*(Se−O) 3c−4e interaction. The interaction aligns the three G- - -Se−O atoms linearly. The G dependence, as well as the O dependence, operates in **2**−**4**. The nonbonded $n_p(G)$- - -σ^*(Se−C) 3c−4e interaction is expected to operate in **2**−**4**, however, the interaction seems very weak in these cases, except for G = Br.

QC calculations are performed on **11**−**14**, the methyl analogues of **1**−**4**. They reproduced the observed structures of **1**−**4**, respectively, and revealed the energy profiles. The energy-lowering effect of the O dependence is estimated to be ca. 20 kJ mol^{-1} and the G dependence of the nonbonded n(Br)- - -σ^*(Se−O) 3c−4e interaction in **14** is close to the value, if the steric repulsion between Br and Se is contained in the G dependence. The G dependence must be larger in an order of F < Cl < Br. On the other hand, the steric repulsion of G also increases in an order of H ≪ F ≪ Cl < Br. The structures of **1**−**5** are explained by above factors.

Studies on the sulfur and tellurium analogues of **1**−**10** are in progress. The results will be reported elsewhere.

Experimental Section

1-(Phenylseleninyl)naphthalene (1a). 1-(Phenylselanyl)naphthalene (**6a**) (100 mg, 0.35 mmol) was dissolved in 20 mL of CH_2Cl_2, and the solution was bubbled through ozone for 15 min. The solution was evaporated and dried in vacuo. The crude product was purified by column chromatography (Al_2O_3, CH_2Cl_2). **1a** was isolated in 65% yield as colorless powder: mp 127.6−129.2 °C (top 128.2 °C, DSC); ^{1}H NMR (400 MHz, $CDCl_3$/TMS) δ 7.35−7.43 (m, 3H), 7.53−7.61 (m, 2H), 7.67 (t, J = 7.7 Hz, 1H), 7.69−7.74 (m, 2H), 7.93 (dd, J = 2.0 and 6.1 Hz, 1H), 7.98 (d, J = 8.2 Hz, 1H), 8.11 (dd, J = 2.3 and 7.1 Hz, 1H), 8.31 (dd, J = 1.0 and 7.3 Hz, 1H); ^{13}C NMR (75 MHz, $CDCl_3$/TMS) δ 122.8, 124.8 (^2J(Se,C) = 8.7 Hz), 126.0, 126.7 (^2J(Se,C) = 14.9 Hz), 126.7, 127.5, 129.1, 129.7, 130.8, 131.2, 131.6, 134.0, 139.2, 142.7; ^{77}Se NMR (76.20 MHz, $CDCl_3$/MeSeMe) δ 840.7. Anal. Calcd for $C_{16}H_{12}OSe$: C, 64.22; H, 4.04. Found: C, 64.01; H, 4.00.

1-(*p*-Benzyloxyphenylseleninyl)naphthalene (1b′). Following the method used for the preparation of **1a**, **1b′** was isolated in 54% yield as colorless prisms: mp 194.6−197.3 °C; ^{1}H NMR (400 MHz, $CDCl_3$/TMS) δ 5.01 (s, 2H), 6.96 (d, J = 8.8 Hz, 2H), 7.28−7.40 (m, 5H), 7.52−7.57 (m, 2H), 7.60 (d, J = 7.0 Hz, 2H), 7.68 (t, J = 7.7 Hz, 1H), 7.90−7.95 (m, 1H), 7.97 (d, J = 8.2 Hz, 1H), 7.99−8.05 (m, 1H), 8.33 (d, J = 7.2 Hz, 1H); ^{13}C NMR (75 MHz, $CDCl_3$/TMS) δ 70.2, 116.0, 122.8, 124.7 (^2J(Se,C) = 8.1 Hz), 126.0, 126.7, 127.4, 127.4, 128.2, 128.7, 128.7, 129.1, 130.7, 131.6, 134.0, 136.1, 161.2; ^{77}Se NMR (76.20 MHz, $CDCl_3$/MeSeMe) δ 839.7 ($\Delta\nu_{1/2}$ = 7.6 Hz). Anal. Calcd for $C_{16}H_{18}O_2Se$: C, 68.15; H, 4.48. Found: C, 68.27; H, 4.63.

1-(*p*-Tolylseleninyl)naphthalene (1d). Following the method used for the preparation of **1a**, **1d** was isolated in 65% yield as colorless prisms: mp 149.1−152.1 °C (top 150.6 °C, DSC); ^{1}H NMR (400 MHz, $CDCl_3$/TMS) δ 2.31 (s, 3H), 7.19 (d, J = 8.0 Hz, 2H), 7.52−7.61 (m, 2H), 7.58 (d, J = 8.4 Hz, 2H), 7.67 (t, J = 7.7 Hz, 1H), 7.90−7.94 (m, 1H), 7.96 (d, J = 8.2 Hz, 1H), 8.03−8.10 (m, 1H), 8.31 (dd, J = 0.9 and 7.3 Hz, 1H); ^{13}C NMR (75 MHz, $CDCl_3$/TMS) δ 21.4, 122.9, 124.7, 126.0, 126.7, 126.7 (^2J(Se,C) = 14.9 Hz), 127.4, 129.1, 130.3, 130.8, 131.5, 134.0, 139.3, 139.5, 141.7; ^{77}Se NMR (76.20 MHz, $CDCl_3$/MeSeMe) δ 839.2 ($\Delta\nu_{1/2}$ = 47.9 Hz). Anal. Calcd for $C_{34}H_{30}O_3Se_2$: C, 63.36; H, 4.69. Found: C, 63.58; H, 4.49.

1-(*p*-Chlorophenylseleninyl)naphthalene (1e). Following the method used for the preparation of **1a**, **1e** was isolated in 69% yield as colorless prisms: mp 142.0−144.3 °C; ^{1}H NMR (400 MHz, $CDCl_3$/TMS) δ 7.37 (d, J = 8.4 Hz, 2H), 7.53−7.63 (m, 2H), 7.65 (d, J = 8.5 Hz 2H),7.67 (t, J = 8.4 Hz, 1H), 7.84 (dd, J = 2.2 and 7.0 Hz, 1H), 7.98 (d, J = 8.2 Hz, 1H), 8.09 (dd, J = 1.0 and 7.1 Hz, 1H), 8.28 (dd, J = 1.0 and 7.3 Hz, 1H); ^{13}C NMR (75 MHz, $CDCl_3$/TMS) δ 122.6, 124.7 (^2J(Se,C) = 8.7 Hz), 126.0, 126.9, 127.7, 127.9 (^2J(Se,C) = 14.9 Hz), 129.3, 129.9, 130.6, 131.8, 134.0, 137.6, 139.0, 141.0; ^{77}Se NMR (76.20 MHz, $CDCl_3$/MeSeMe) δ 840.5 ($\Delta\nu_{1/2}$ = 9.8 Hz). Anal. Calcd for $C_{16}H_{11}ClOSe$: C, 57.59; H, 3.32. Found: C, 57.31; H, 3.32.

1-(*p*-Nitrophenylseleninyl)naphthalene (1f). Following the method used for the preparation of **1a**, **1f** was isolated in 76% yield as light yellow prisms: mp 162.0−164.1 °C (top 163.1 °C, DCS); ^{1}H NMR (400 MHz, $CDCl_3$/TMS) δ 7.57−7.70 (m, 3H), 7.91−7.99 (m, 3H), 8.01 (d, J = 8.3 Hz, 1H) 8.16 (d, J = 7.5 Hz, 1H), 8.24 (d, 3H); ^{13}C NMR (75 MHz, $CDCl_3$/TMS) δ 122.3, 124.5, 124.8, 126.1, 127.1, 127.4 (^2J(Se,C) = 13.1 Hz), 128.0, 129.4, 130.6, 132.2, 134.1, 138.7, 149.6, 150.1; ^{77}Se NMR (76.20 MHz, $CDCl_3$/MeSeMe) δ 842.9 ($\Delta\nu_{1/2}$ = 15.3 Hz). Anal. Calcd for $C_{16}H_{11}NO_3Se$: C, 55.83; H, 3.22; N, 4.07. Found: C, 55.90; H, 3.22; N, 4.16.

8-Fluoro-1-(*p*-anisylseleninyl)naphthalene (2b). Following the method used for the preparation of **1a**, **2b** was isolated in 50% yield as colorless prisms: mp 140.0−142.5 °C; ^{1}H NMR (400 MHz, $CDCl_3$/TMS) δ 3.74 (s, 3H), 6.85 (d, J = 8.6 Hz, 2H), 7.24 (t, J = 6.2 Hz, 1H), 7.45 (dd, J = 7.9 and 13.6 Hz, 1H), 7.60 (d, J = 8.8 Hz, 2H), 7.72 (d, J = 8.2 Hz, 1H), 7.77 (t, J = 7.7 Hz, 1H), 7.96 (d, J = 8.1 Hz, 1H), 8.69 (d, J = 7.3 Hz, 1H); ^{13}C NMR (75 MHz, $CDCl_3$/TMS) δ 55.4, 111.7 (^2J(F,C) = 20.6 Hz), 114.9, 115.2, 124.2, 125.1 (^3J(F,C) = 3.7 Hz), 126.4 (^2J(F,C) = 8.7 Hz), 127.0 (^4J(F,C) = 1.9 Hz), 128.5 (^6J(F,C) = 2.5 Hz, ^2J(Se,C) = 11.2 Hz), 128.6, 130.8 (^3J(F,C) = 2.8 Hz), 135.3, 135.9 (^2J(F,C) = 5.9 Hz), 158.2 (^1J(F,C) = 250.1 Hz), 162.1; ^{77}Se NMR (76.20 MHz, $CDCl_3$/MeSeMe) δ 862.1 (^4J(Se,F) = 218.5 Hz). Anal. Calcd for $C_{17}H_{13}FO_2Se$: C, 58.80; H, 3.77. Found: C, 58.95; H, 3.94.

8-Chloro-1-(*p*-*tert*-butylphenylseleninyl)naphthalene (3c). Following the method used for the preparation of **1a**, **3c** was isolated in 58% yield as colorless prisms: mp 178.5−179.8 °C (top 179.4 °C, DSC); ^{1}H NMR (400 MHz, $CDCl_3$/TMS) δ 1.23 (s, 9H), 7.34 (d, J = 8.3 Hz, 2H), 7.45 (t, J = 8.0 Hz, 1H), 7.51 (d, J = 8.0 Hz, 2H), 7.62 (d, J = 7.8 Hz, 1H), 7.80 (t, J = 7.8 Hz, 1H), 7.89 (d, J = 8.3 Hz, 1H), 8.01 (d, J = 8.3 Hz, 1H), 8.95 (d, J = 7.8 Hz, 1H); ^{13}C NMR (75 MHz, $CDCl_3$/TMS) δ 31.1, 34.8, 126.3, 126.5, 126.7, 126.7, 127.1 (^2J(Se,C) = 13.1 Hz), 128.7, 128.8, 129.1, 129.7, 132.2, 136.4, 139.4, 142.3, 154.1; ^{77}Se NMR (76.20 MHz, $CDCl_3$/MeSeMe) δ 867.4 ($\Delta\nu_{1/2}$ = 4.9 Hz). Anal. Calcd for $C_{20}H_{19}ClOSe$: C, 61.63; H, 4.91. Found: C, 61.36; H, 4.81.

8-Chloro-1-(*p*-chlorophenylseleninyl)naphthalene (3e). Following the method used for the preparation of **1a**, **3e** was isolated in 69% yield as colorless prisms: mp 171.3−173.4 °C (top 172.8 °C, DSC); ^{1}H NMR (400 MHz, $CDCl_3$/TMS) δ 7.30 (d, J = 8.5 Hz, 2H), 7.47 (t, J = 7.8 Hz, 1H), 7.58 (d, J = 8.5 Hz, 2H), 7.64 (dd, J = 1.1 and 7.5 Hz, 1H), 7.79 (t, J = 7.8 Hz,1H), 7.90 (dd, J = 0.9 and 8.2 Hz, 1H), 8.02 (dd, J = 0.9 and 8.2 Hz, 1H), 8.91 (dd, J = 1.2 and 7.4 Hz, 1H);^{13}C NMR (75 MHz, $CDCl_3$/TMS) δ 126.3, 126.5, 126.7, 128.4, 128.6 (^2J(Se,C) = 13.7 Hz), 128.9, 129.2, 129.3, 129.5, 132.5, 136.4, 136.9, 139.3, 143.7; ^{77}Se NMR (76.20 MHz, $CDCl_3$/MeSeMe) δ 866.2 ($\Delta\nu_{1/2}$ = 5.6 Hz). Anal. Calcd for $C_{16}H_{10}Cl_2OSe$: C, 52.20; H, 2.74. Found: C, 52.03; H, 2.74.

8-Bromo-1-(*p*-anisylseleninyl)naphthalene (4b). Following the method used for the preparation of **1a**, **4b** was isolated in 77% yield as colorless prisms: mp 132.1−134.4 °C (top 133.5 °C, DSC); ^{1}H NMR (400 MHz, $CDCl_3$/TMS) δ 3.74 (s, 3H), 6.81 (d, J = 8.6 Hz, 2H), 7.37 (t, J = 7.8 Hz, 1H), 7.49 (d, J = 8.5 Hz, 2H), 7.79 (t, J = 7.7 Hz, 1H), 7.84 (d, J = 7.5 Hz, 1H), 7.94 (d, J = 8.1 Hz,,1H), 8.00 (d, J = 8.1 Hz, 1H), 8.99 (d, J = 7.4 Hz, 1H); ^{13}C NMR (75 MHz, $CDCl_3$/TMS) δ 55.4, 114.8, 118.7, 126.6, 126.7, 127.1, 129.3 (^2J(Se,C) = 14.3 Hz), 129.5, 130.2, 132.5, 133.4, 136.6, 136.9, 140.3, 161.3; ^{77}Se NMR (76.20 MHz, $CDCl_3$/MeSeMe) δ 863.6 ($\Delta\nu_{1/2}$ = 5.5 Hz). Anal. Calcd for $C_{17}H_{15}BrO_3Se$: C, 47.91; H, 3.55. Found: C, 48.15; H, 3.61.

1,1′-Dinaphthyl Selenoxide (5). Following the method used for the preparation of **1a**, **5** was isolated in 87% yield as colorless prisms: mp 181.2−183.2 °C (top 182.2 °C, DSC); ^{1}H NMR (400 MHz, $CDCl_3$/TMS) δ 7.49−7.62 (m, 4H), 7.58 (t, J = 7.7 Hz, 2H), 7.90 (dd, J = 2.1 and 7.0 Hz, 2H), 7.94 (d, J = 8.1 Hz, 2H), 8.15 (d, J = 7.3 Hz, 2H), 8.24 (dd, J = 1.6 and 7.4 Hz, 2H); ^{13}C NMR (75 MHz, $CDCl_3$/TMS) δ 123.2 (^2J(Se,C) = 14.9 Hz), 126.0, 126.4, 126.7, 127.7, 129.1, 131.1, 131.8, 133.9, 139.3; ^{77}Se NMR (76.20 MHz, $CDCl_3$/MeSeMe) δ 826.9 ($\Delta\nu_{1/2}$ = 10.5 Hz). Anal. Calcd for $C_{20}H_{14}OSe$: C, 68.77; H, 4.04. Found: C, 68.53; H, 4.05.

1-(*p*-Benzyloxyphenylselanyl)naphthalene (6b′). Under an argon atmosphere, 1-bromonaphthalene (1.52 g, 7.34 mmol) was dissolved in 25 mL of dry THF, and the solution was added to *n*-BuLi (4.7 mL, 7.61 mmol, 1.5 N) at −78 °C. After 50 min, a THF solution of *p*- benzyloxyphenylselenobromide was added to the above solution at −78 °C. The reaction mixture was stirred for 2 h and warmed until a cloudy mixture resulted. Then, 20 mL of 5% acetone hydrochloric acid and 100 mL of benzene were added. The organic layer was separated and washed with brine, 10% aqueous solution of sodium hydroxide, saturated aqueous solution of sodium bicarbonate, and brine. The solution was dried over sodium sulfate, evaporated, and dried in vacuo. The crude product was purified by column chromatography (SiO_2, hexane). Compound **6b′** was isolated in 67% yield as colorless prisms: mp 109.9−111.7 °C (top 110.6 °C, DSC); ^{1}H NMR (400 MHz, $CDCl_3$/TMS) δ 5.04 (s, 2H), 6.89 (d, J = 8.5 Hz, 2H), 7.23−7.58 (m, 11H), 7.76 (d, J = 8.2 Hz, 1H), 7.83 (d, J = 7.4 Hz, 1H), 8.28 (d, J = 8.5 Hz, 1H); ^{13}C NMR (75 MHz, $CDCl_3$/TMS) δ 70.1, 116.1, 120.6, 126.0, 126.2, 126.6, 126.9, 127.5, 128.0, 128.1, 128.5, 128.6, 131.1, 131.5, 133.3, 134.0, 135.5, 136.7, 158.7; ^{77}Se NMR (76.20 MHz, $CDCl_3$/MeSeMe) δ 354.6. Anal. Calcd for $C_{23}H_{18}OSe$: C, 70.95; H, 4.66. Found: C, 71.06; H, 4.58.

8-Chloro-1-(*p*-*tert*-butylphenylselanyl)naphthalene (8c). Following the method used for the preparation of **6b′**, **8c** was isolated in 67% yield as colorless prisms: mp 128.0−129.0 °C (top 128.7 °C, DSC); ^{1}H NMR (400 MHz, $CDCl_3$/TMS) δ 1.36 (s, 9H), 7.12 (t, J = 7.7 Hz, 1H), 7.23 (dd, J = 0.5 and 8.4 Hz, 1H), 7.32 (t, J = 7.8 Hz, 1H), 7.43 (dd, J = 2.0 and 8.4 Hz, 2H), 7.56−7.62 (m, 4H), 7.72 (dd, J = 1.3 and 8.2 Hz, 1H); ^{13}C NMR (75 MHz, $CDCl_3$/TMS) δ 31.3, 34.8, 125.6, 126.4, 126.7, 127.0, 127.1, 128.5, 128.8, 129.3, 130.0, 131.7, 133.2, 136.9 (^2J(Se,C) = 11.2 Hz), 136.9, 152.3; ^{77}Se NMR (76.20 MHz, $CDCl_3$/MeSeMe) δ 448.9. Anal. Calcd for $C_{20}H_{19}ClSe$: C, 64.27; H, 5.12. Found: C, 64.05; H, 5.17.

8-Bromo-1-(*p*-*tert*-butylphenylselanyl)naphthalene (9c). Following the method used for the preparation of **6b′**, **9c** was isolated in 64% yield as colorless prisms: mp 127.3−128.4 °C (top 128.0 °C, DSC); ^{1}H NMR (400 MHz, $CDCl_3$/TMS) δ 1.48 (s, 9H), 7.24 (t, J = 7.5 Hz, 1H), 7.35 (dd, J = 1.3 and 8.8 Hz, 1H), 7.37 (t, J = 5.1 Hz, 1H), 7.53 (dt, J = 2.1 and 8.6 Hz, 2H), 7.69 (dt, J = 1.6 Hz and 8.2 Hz, 2H), 7.72 (dd, J 1.3 and 8.4 Hz, 1H), 7.89 (dd, J = 1.2 and 8.2 Hz, 1H), 7.96 (dd, J = 1.3 and 7.5 Hz, 1H); ^{13}C NMR (75 MHz, $CDCl_3$/TMS) δ 31.3, 34.7, 120.4, 126.0, 126.3, 127.0, 127.2, 128.2, 129.2, 130.4, 131.5, 133.2, 133.7, 136.6 (^2J(Se,C) = 11.2 Hz), 137.0, 152.1; ^{77}Se NMR (76.20 MHz, $CDCl_3$/MeSeMe) δ 442.9. Anal. Calcd for $C_{20}H_{19}BrSe$: C, 57.44; H, 4.58. Found: C, 57.22; H, 4.50.

1,1′-Dinaphthyl Selenide (10). Following the method used for the preparation of **6b′**, **10** was isolated in 71% yield as colorless prisms, mp 99.8−103.2 °C (top 101.1 °C, DSC); ^{1}H NMR (300 MHz, $CDCl_3$/TMS) δ 7.27 (t, J = 7.1 Hz, 2H), 7.48 (dd, J = 1.0 and 7.2 Hz, 2H), 7.50−7.55 (m, 4H), 7.79 (d, J = 8.0, 2H), 7.83−7.88 (m, 2H), 8.30−8.36 (m, 2H); ^{13}C NMR (75 MHz, $CDCl_3$/TMS) δ 126.1, 126.3, 126.8, 127.1 (^2J(Se,C) = 14.3 Hz), 128.4, 128.6, 129.8, 132.2 (^3J(Se,C) = 6.2 Hz), 133.6, 134.1; ^{77}Se NMR (76.20 MHz, $CDCl_3$/MeSeMe) δ 310.7. Anal. Calcd for $C_{20}H_{14}Se$: C, 72.07; H, 4.23. Found: C, 72.11; H, 4.27.

X-ray Structural Determination of 1a, 1b′, 1d, 1e, 1f, 2b, 3c, 3e, 4b, 5, and 10. The colorless crystals of **1a**, **1b′**, **1d**, **1e**, **1f**, **2b**, **3c**, **3e**, **4b**, **5**, and **10** were grown by slow evaporation of dichloromethane-hexane solutions at room temperature. The intensity data were collected on a CCD diffractometer equipped with graphite-monochromed Mo Kα irradiation (λ = 0.71070 Å) at 103(2) K for **1a** and **4b** and on a four-circle diffractometer with graphite-monochromated Mo Kα radiation (λ = 0.71069 Å) for **1b′**, **1d**, **1e**, **1f**, **2b**, **3c**, **3e**, **5**, and **10** at 298(1) K. The structures of **1a** and **4b** were solved by direct methods (SIR97)[30] and DIRDIF99 (PATTY),[31] respectively, and refined by full-matrix least-squares methods on F^2 for all reflections (SHELXL-97).[32] The structures of **1b′**, **1d**, **1f**, **2b**, **3c**, **3e**, **5**, and **10** were solved by heavy-atom Patterson methods, PATTY,[33] and SAPI91[34] for **1e** and expanded using Fourier techniques, DIRDIF94.[35] All of the non-hydrogen atoms were refined anisotropically. Crystallographic details are given in the Supporting Information.

MO Calculations. Quantum chemical (QC) calculations were performed with the 6-311+G(2d, p) and/or 6-311+G(d) basis sets of the Gaussian 98 program.[19] Calculations are performed at the density functional theory (DFT) level of the Becke three parameter hybrid functional combined with the Lee−Yang−Parr correlation

(30) Altomare, A.; Burla, M. C.; Camalli, M.; Cascarano, G.; Giacovazo, C.; Gualgliardi, A.; Moliterni, A. G. G.; Polidori, G.; Spagna, R. *J. Appl. Crystallogr.* **1999**, *32*, 115−119.

(31) Beurskens, P. T.; Admiraal, G.; Beurskens, G.; Bosman, W. P.; de Gelder, R.; Israel, R.; Smits, J. M. M. *The DIRDIF-99 Program System, Technical Report of the Crystallography Laboratory*; University of Nijmegen, The Netherlands, 1999.

(32) Sheldrick, G. M. *SHELXL-97, Program for the Refinement of Crystal Structures*; University of Göttingen: Göttingen, 1997.

(33) Beurskens, P. T.; Admiraal, G.; Beurskens, G.; Bosman, W. P.; Garcia-Granda, S.; Gould, R. O.; Smits, J. M. M.; Smykalla, C. *DIRDIF92, The DIRDIF program system*, Technical Report of the Crystallography Laboratory; University of Nijmegen: The Netherlands, 1992.

(34) Hai-Fu, F. SAPI91, *Structure Analysis Programs with Intelligent Control*; Rigaku Corp.: Tokyo, 1991.

(35) Beurskens, P. T.; Admiraal, G.; Beurskens, G.; Bosman, W. P.; de Gelder, R.; Israel, R.; Smits, J. M. M. *The DIRDIF-94 program system, Technical Report of the Crystallography Laboratory*; University of Nijmegen: The Netherlands, 1994.

(36) (a) Lias, S. G.; Bartmess, J. E.; Holmes, J. L.; Levin, R. D.; Liebman, J. F.; Mallard, W. G. Gas-Phase Ion and Newtral Thermochemistry. *J. Phys. Chem. Ref. Data*, *17*, *Suppl.* **1988**, 1. (b) Jordan, K. D.; Burrow, P. D. *Acc. Chem. Res.* **1978**, *11*, 341−348. (c) Jordan, K. D.; Burrow, P. D. *Chem. Res.* **1987**, *87*, 557−588.

(37) Nakanishi, W.; Hayashi, S. unpublished results.

functional (B3LYP). Optimized structures and the molecular orbitals are drawn using MolStudio R3.2 (Rev 1.0).[23]

Acknowledgment. We are grateful to Prof. Norihiro Tokitoh and Dr. Takahiro Sasamori, Institute for Chemical Research, Kyoto University, for the X-ray diffraction measurements of **1a** and **4b**. This work was partially supported by a Grant-in-Aid for Scientific Research (No. 16550038) from the Ministry of Education, Culture, Sports, Science, and Technology, Japan.

Supporting Information Available: General experimental details; X-ray crystallographic data for **1a**, **1b′**, **1d**, **1e**, **1f**, **2b**, **3c**, **3e**, **4b**, **5**, and **10** (CIF); ORTEP structures of **1d**, **1f**, and **3c**; optimized structures given by Cartesian coordinates for **11**−**14** and **11**•H^+, together with the total energies and the method for the calculations. This material is available free of charge via the Internet at http://pubs.acs.org.

JO060527F